Distribution Transformer Incipient Fault Automatic Detection and Monitoring

Guilherme Rodrigues Freire
guilhermerfreire@tecnico.ulisboa.pt

Instituto Superior Técnico, Lisboa, Portugal

October 2020

Abstract

Transformers are one of the most essential and expensive components of electric grids. Recently, concern with incipient fault detection is growing due to the large amount of transformers currently in service reaching the end of their designated lifespan. This work presents a computational and experimental study of a set of electrical and magnetic variables. Simulation results are applied to the development of a potential incipient fault detection and localization methodology for distribution transformers. Subsequently, analysis of a smaller scale experimental setup is used to assess the scalability of the proposed methods regarding the rated power of the transformer.
Keywords: Distribution transformer, On-line monitoring, Incipient faults, Detection, Localization

1. Introduction

It is widely established that power transformers are one of the most critical and expensive components in electric grids [1] [2] [3] [4]. In particular, distribution transformers comprise the ultimate interface between the grid and the consumer. Failure of such equipment can imply high costs, either due to repairs or system unavailability [1].

There is a large number of transformers which have been in service for a significant amount of time and is currently reaching the end of designated lifespan. Figure 1 shows the age statistics for ENW (Electricity North West) distribution transformers (reportedly over 30000 units) up until 2015 [5]. The data suggests that over 40% of the distribution transformers managed by ENW were over 40 years old.

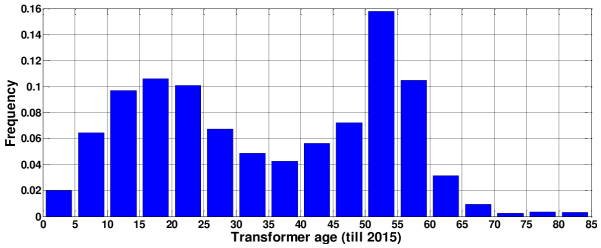

Figure 1: Age profile of a population of over 30000 ENW distribution transformers until 2015, published in [5].

With this paradigm comes a growing concern with the health condition of currently servicing transformers. Consequently, transformer monitoring has become a priority for utilities, in an effort to avoid accidental losses.

Transformer monitoring techniques can be divided into two main categories: on-line and off-line. Off-line methods require the transformer to be taken off service for inspection. In this category, one should highlight the following methodologies:

- Dissolved gas analysis (DGA) [6];
- Furan analysis [7];
- Winding resistance and turn ratio measurements [8] [9] [10];
- Dissipation factor test [11];
- Leakage reactance measurement [11];
- Frequency response analysis [11].

On the other hand, on-line techniques allow the operator to continuously monitor the transformer while it is in service, which is why such methods are more desirable. Important on-line monitoring methodologies include:

- Electrical methods [12] [13] [14];
- Partial discharge detection [15];
- Thermal monitoring [16] [17] [18] [19] [20];
- Vibro-acoustic monitoring [3] [21] [22].

Figure 2 [23] provides a statistical analysis on transformer failures. From this data, one readily concludes that, for distribution transformers, winding failures are by far the most common. Therefore, incipient winding faults will be the main focus of the simulations and experimental procedure presented in this work.

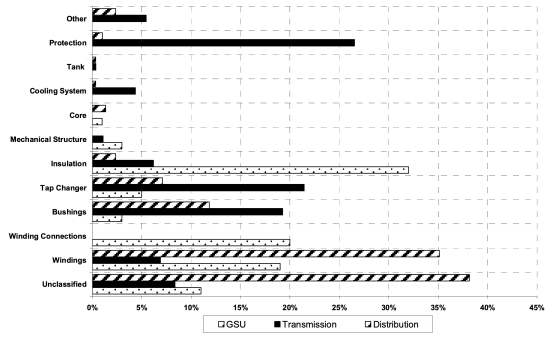

Figure 2: Transformer failure location statistics for GSU, transmission and distribution transformers, as published in [23].

This work provides a computational and experimental study of a potential incipient winding fault detection and localization methodology. In the following section (2), the theoretical background is given. Thereafter, section 3 discusses the implementation of the simulation model and experimental setup. The results obtained from those are then analyzed in section 4 and, finally, the main conclusions and guidelines for future work are listed in section 5.

2. Theoretical Background

2.1. Fortescue transformation and symmetrical components

The Fortescue transformation is a tool for three-phase system analysis. It allows one to simplify analysis by decomposing the three-phase system, balanced or unbalanced, into three independent balanced systems. Mathematically, it is a complex linear transformation given by eq. (1), where α is a complex 120° rotation coefficient.

$$\mathbf{T_F} = \begin{bmatrix} 1 & 1 & 1 \\ \alpha^2 & \alpha & 1 \\ \alpha & \alpha^2 & 1 \end{bmatrix} \qquad \alpha = e^{j\frac{2\pi}{3}} \tag{1}$$

In transformers, to account for the primary and secondary windings, a global transformation matrix can be defined - eq. (2) [24].

$$\mathbf{T_F^g} = \begin{bmatrix} \mathbf{T_F} & \mathbf{0} \\ \mathbf{0} & \mathbf{T_F} \end{bmatrix} \tag{2}$$

Making use of eq. (2), the line voltages and currents in the transformer can be decomposed into their symmetrical component systems - eqs. (3) and (4).

$$\mathbf{V_{dih}^g} = \left(\mathbf{T_F^g}\right)^{-1} \mathbf{V_{abc}^g} \tag{3}$$

$$\mathbf{I_{dih}^g} = \left(\mathbf{T_F^g}\right)^{-1} \mathbf{I_{abc}^g} \tag{4}$$

2.2. Frequency domain analysis

Generally, electromagnetic systems are analyzed according to the time-harmonic Maxwell's equations. However, a simplification can be performed, in which all quantities are assumed to be approximately sinusoidal, in which case the problem can be reduced to the frequency domain formulation of Maxwell-Ampère's law - eq. (5) which can then be solved computationally resorting to finite element method (FEM) [25].

$$\begin{aligned} \left(j\omega\sigma - \omega^2\varepsilon_0\right)\mathbf{A} + \nabla \times \left(\frac{1}{\mu_0}\nabla \times \mathbf{A} - \mathbf{M}\right) \\ -\sigma\mathbf{v} \times (\nabla \times \mathbf{A}) = \mathbf{J}_e \end{aligned} \tag{5}$$

2.3. Effective B-H curve

Ferromagnetic materials are typically represented by a non-linear B-H magnetization curve. However, in frequency domain analysis, an effective B-H curve approximation can be used, since all quantities are assumed to be sinusoidal. The preferred curve transformation method is analogous to the Average Energy Method [26], which is invariant with respect to the average magnetic energy density. The effective B-H curve relates the RMS values of an imposed sinusoidal $B\,(t)$ and an equivalent sinusoidal $H_{eq}\,(t)$ which preserves the average magnetic energy density yielded by the actual magnetic field $H\,(t)$. These quantities are mathematically defined according to eqs. (6) - (8). Figure 3 shows the effective B-H curve of the 35PN300 Silicon Steel (non grain-oriented) used in the FEM simulation model.

$$B\,(t) = B_{eff}\sqrt{2}\sin\left(2\pi f t\right) \tag{6}$$

$$H_{eq}\,(t) = H_{eff}\sqrt{2}\sin\left(2\pi f t\right) \tag{7}$$

$$H_{eff} = \frac{1}{B}\frac{8}{T}\int_0^{\frac{T}{4}}\left(\int_{B(0)}^{B(t)} H(B)dB\right)dt \tag{8}$$

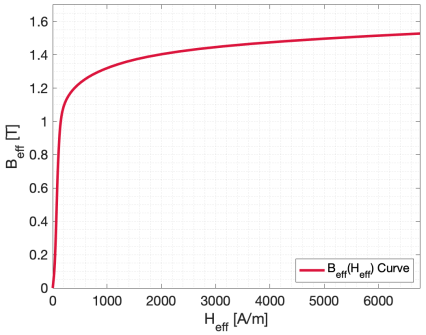

Figure 3: Effective B-H curve of the 35PN300 Silicon Steel (NGO)

2.4. Analytical model

An analytical model of the transformer was developed as to establish a base for comparison for the FEM simulation model. This model is based on:

- The single-phase equivalent circuit of the transformer, which was used to establish transformer behavior during open-circuit and short-circuit tests;
- The inductance matrix of the transformer - defined by eqs. (9) - (10) - specifically the self-inductances of the primary and secondary coils.

$$x = \frac{\mu(H)\,S}{2l_h + 3l_v} \qquad y = \frac{l_h + l_v}{2l_h + l_v} \qquad z = \frac{l_v}{2l_h + l_v} \tag{9}$$

$$\begin{bmatrix} A & B & C \\ D & E & F \\ G & H & I \end{bmatrix} = x \begin{bmatrix} 2yN_p^2 & 2N_p^2 & zN_p^2 \\ 2yN_pN_s & 2N_pN_s & zN_pN_s \\ 2yN_s^2 & 2N_s^2 & zN_s^2 \end{bmatrix} \tag{10}$$

$$\mathbf{L} = \begin{bmatrix} A & -\frac{1}{2}B & -C & D & -\frac{1}{2}E & -F \\ -\frac{1}{2}B & B & -\frac{1}{2}B & -\frac{1}{2}E & E & -\frac{1}{2}E \\ -C & -\frac{1}{2}B & A & -F & -\frac{1}{2}B & D \\ D & -\frac{1}{2}E & -F & G & -\frac{1}{2}H & -I \\ -\frac{1}{2}E & E & -\frac{1}{2}E & -\frac{1}{2}H & H & -\frac{1}{2}H \\ -F & -\frac{1}{2}B & D & -I & -\frac{1}{2}H & G \end{bmatrix} \tag{11}$$

3. Implementation

3.1. Simulation Model

A simulation model of a 15/0.4kV, 690kVA, three-phase, delta-wye connected distribution transformer was developed resorting to a FEM software. Figures 4, 5 and 6 show the model geometry, mesh and electrical circuits, respectively. The depth of the 2D model was taken to be the thickness of the transformer (175mm). The transformer core is made of 35PN300 Silicon Steel (NGO), the windings are defined as homogenized copper coils and the space around the transformer is air. The primary coils are each comprised of 1300 turns, and the secondary has 20 turns per phase. The outer layer of the mesh is defined as an infinite element domain, in which field decay is exponential.

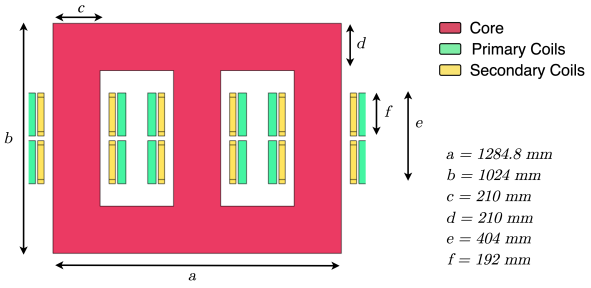

Figure 4: Model geometry (core and windings), with highlighted parts and measurements. Note: domains surrounding core and windings are hidden.

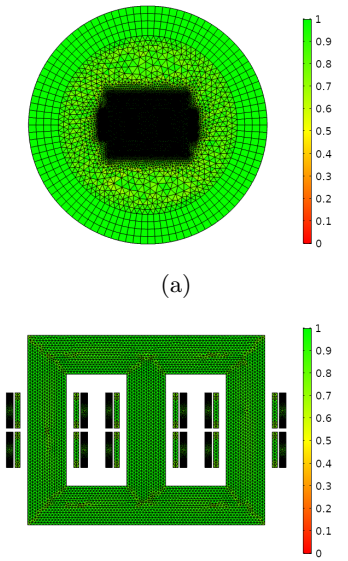

(a)

(b)

Figure 5: Model mesh: (a) global view of mesh; (b) detail of interest region (core and windings).

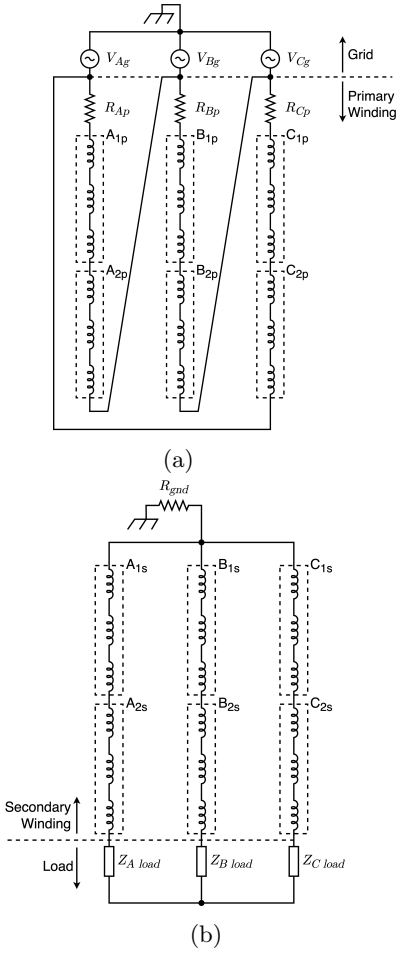

(a)

(b)

Figure 6: Lumped parameter electrical circuits: (a) primary; (b) secondary.

The FEM model was validated according to the analytical model defined in section 2.4 and was verified to be working correctly. It was then used to perform a total of 3240 frequency domain simulations which emulate gradual incipient winding faults. Gradual losses of 1, 2 and 3 turns were tested in the primary and secondary windings, for 5 different vertical locations in each phase, by varying the value of a resistor connected in parallel with the faulty turns. The connection diagram of fig. 7 corresponds to an example for a gradual loss of a single turn. The value of R_{stl} in each simulation is computed according to eq. (12), where R_{1t} is the resistance of one turn and p is the portion of the turn resistance that is lost.

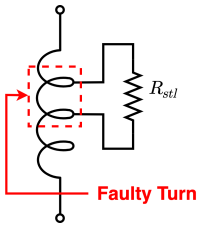

Figure 7: Generic connection scheme for simulation of a gradual single turn loss.

$$R_{stl} = \frac{1-p}{p} R_{1t} \tag{12}$$

3.2. Experimental Setup

The experimental setup uses a small 400V, 4kVA, three-phase, delta-wye connected, air-cooled power transformer. Each phase has 5 independent 52V secondary windings. A connection and enclosure system comprised of two connection boards and a wooden case was built. The finalized experimental setup is represented in fig. 8.

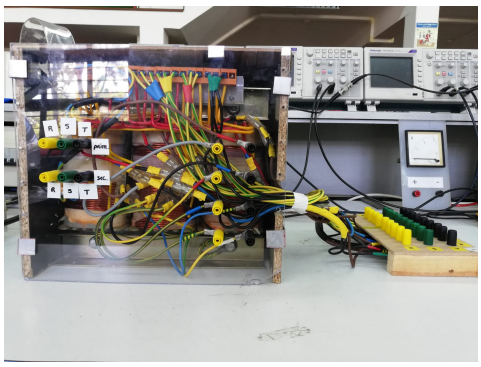

Figure 8: Final experimental setup used for experimental emulation of incipient winding faults.

Figure 9 shows the main connection board (board 1), where the fault emulation terminals were created by performing adjustments (cuts) on four distinct turns in one of the secondary windings in phase B (middle limb). The altered turns were then rerouted to the connection board according to the schematic of fig.10.

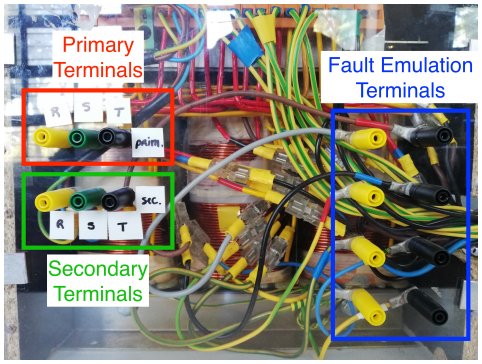

Figure 9: Main connection board (board 1) of the experimental setup.

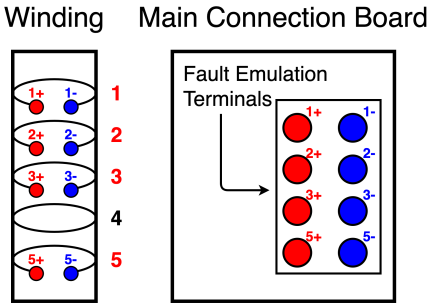

Figure 10: Schematic representation of fault emulation terminals connection diagram.

A secondary connection board (board 2) was built to allow the series connection of the independent secondaries in each phase, making a single 260V secondary winding per phase. Figure 11 shows a top and bottom view of the secondary connection board.

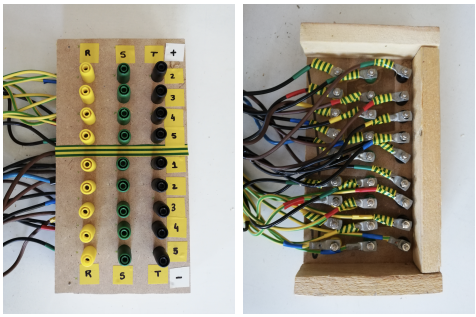

(a) (b)

Figure 11: Top (a) and bottom (b) view of the custom connection board (board 2) for the multiple secondary terminals.

The experimental setup was tested by performing open-circuit, short-circuit and rated load tests and was verified to be operating as expected. It was then used to emulate several winding faults in phase B, middle limb. The connection diagrams of the fault emulation terminals for each test are shown in fig. 12.

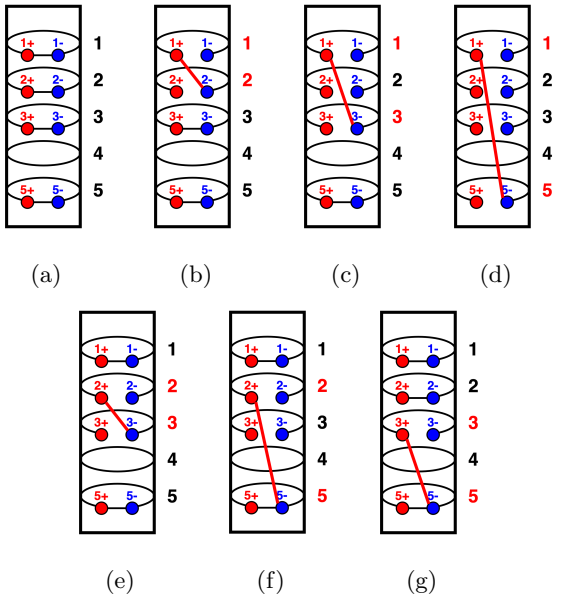

Figure 12: Connection diagrams for the fault emulation tests: (a) Reference; (b) 1 - 2; (c); 1 - 3; (d) 1 - 5; (e) 2 - 3; (f) 2 - 5; (g) 3 - 5.

4. Results

4.1. Simulation

The simulation model described in section 3.1 was used to study the behavior of the line voltages and currents and their symmetrical components, as well as the magnetic flux density distribution and flux leakage in the presence of incipient winding faults. The results were compared for 5 different fault locations within each phase, in the primary and secondary windings. For simplicity, the case of a gradual single turn loss fault in phase B of the secondary winding will be taken as reference, and analysis of the remaining cases will be reduced to comparative methods. Figures 13, 14 and 15 show the results obtained for the variations in line voltages and currents, positive (D) and negative (I) sequence components of the line currents and the average magnetic flux leakage to either side of the middle limb, respectively, depending on fault severity and location.

From fig. 13, one can conclude that the line voltage and current in the faulty phase drop as the fault becomes more severe. Said decrease is more significant when the fault happens in the middle section of the coil than in the top or bottom extremities,

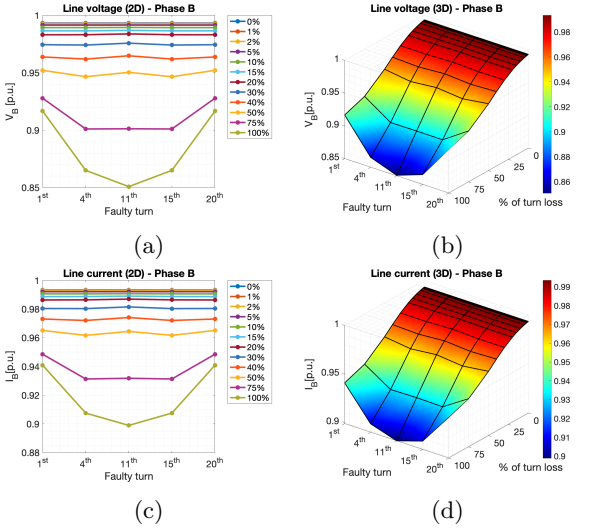

Figure 13: Variation of the line voltages and currents according to fault location and severity: (a) voltage, 2D; (b) voltage, 3D; (c) current, 2D; (d) current, 3D. Fault located in phase B.

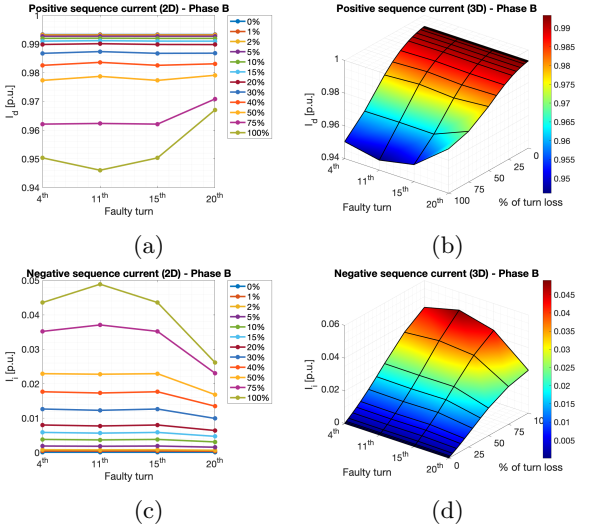

Figure 14: Variation of the positive and negative sequence currents according to fault location and severity: (a) positive, 2D; (b) positive, 3D; (c) negative, 2D; (d) negative, 3D. Fault located in phase B.

i.e., the curves are symmetrical with respect to the middle section.

The positive sequence current also drops as the fault progresses. This decrease is accompanied by a rise in negative sequence current, which was virtually non-existent at first. This can be seen in fig. 14. Here it is important to note that the results for a fault in the 1st turn have been excluded due to it being a special case, in which a zero sequence component appears, which leads to a more numerically significant drop in positive sequence and rise in neg-

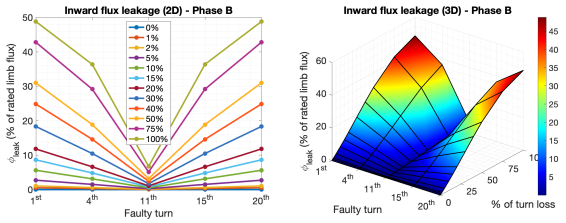

(a) (b)

Figure 15: Variation of inward flux leakage according to fault location and severity: (a) 2D; (b) 3D. Fault located in phase B.

ative sequence currents. This is a consequence of the grounding scheme of the modeled transformer (see fig. 6. This makes the positive and negative sequence currents the only group of variables studied in this work capable of distinguishing faults in the top and bottom sections of the coil, since the curves are not symmetrical with respect to the middle section.

The magnetic flux leakage curves, represented in fig. 15 make a clear distinction between faults in the middle section and extremities of the coil, since leakage flux re-entry happens for faults in the middle section due to the higher distance to the horizontal chunks of the core.

The same qualitative conclusions apply when the faults occur in phases A or C, although the flux leakage to either side of the faulty limb is not exactly symmetrical due to magnetic circuit topology.

For single turn loss faults in the primary winding, the variations are much less significant numerically speaking. In the case of the electrical variables, variations might even be too slight to distinguish conclusively. However, the qualitative conclusions taken for the secondary still apply, with the exception of the asymmetry of the positive and negative sequence current curves. Since the primary is delta-connected, the zero sequence current is always null, and the variations in the remaining symmetrical components are numerically indistinguishable when faults occur in the top and bottom sections of the core.

When faults involve more than one turn (simulations were performed for 2 and 3 turn faults), although the variations are in general more numerically significant, all the qualitative conclusions taken for single turn faults hold true. Nevertheless, it is important to add:

1. In the primary, the increase in numerical significance increases the ability to detect and locate faults;

2. In the secondary, the demagnetization of the core becomes so strong that the increase of the flux leakage with fault severity becomes less than linear.

In order to confirm the accuracy of the model, the magnetic flux density distribution obtained through frequency domain analysis was compared to more exact time domain simulations - fig. 16(a). The same comparison was made for time domain results with and without harmonics (odd harmonics up to the 9^{th}) - fig. 16(b). Results allow one to conclude that the deviation in the interest region of the core is very low, which indicates the results obtained through frequency domain simulations should hold true even in the presence of harmonics.

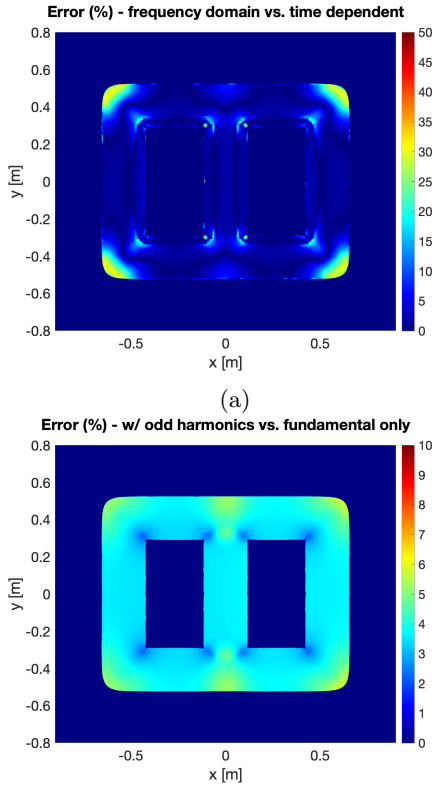

(a)

(b)

Figure 16: Magnetic flux density deviation, at rated voltage and load: (a) frequency domain vs. time domain; (b) with harmonics vs. purely sinusoidal.

Finally, a potential methodology for incipient winding fault detection and localization based on the simulation results is proposed - fig. 17. Note that this methodology is valid for the secondary winding. However, in the primary, the final step that allows one to distinguish between faults in the top and bottom sections of the coil based on the numerical significance of the variations in the symmetrical components of the current is not feasible, due to its delta connection.

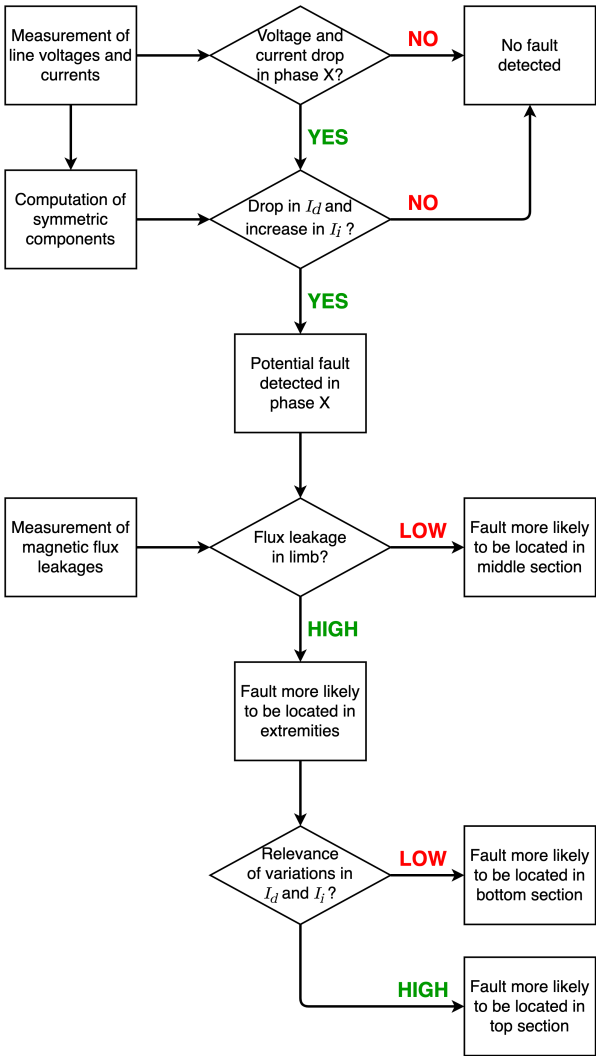

Figure 17: Flowchart of the proposed fault detection and localization methodology, for a fault in phase X of the secondary winding.

4.2. Experimental

The experimental setup described in section 3.2 was to perform the incipient winding fault emulation tests corresponding to the diagrams of fig. 12. Taking a rated load test as the reference, the variations in the voltages and currents, as well as their symmetrical components, were registered in tables 1 and 2 , respectively.

The results of tabs. 1 and 2 should be analyzed in terms of variation trends, rather than numerically. For all intended purposes, "variation trend" a monotonic increase or decrease of an interest variable with respect to its reference value.

Taking only the variables that show such variation trends, one can elaborate a fault severity rating table (tab. 3) according to each variable. To that end, a reference ranking (first row of tab. 3) should be defined, according to the following criteria:

Table 1: Experimental results for line voltages and currents on primary and secondary side - variations with respect to rated load test (reference).

Number of Lost Turns		1		2		3	4
Test		1 - 2	2 - 3	1 - 3	3 - 5	2 - 5	1 - 5
V_p	A	-0.03%	-0.28%	-0.29%	-0.26%	-0.12%	-0.26%
	B	+0.16%	-0.53%	-0.20%	-0.41%	-0.39%	+0.27%
	C	-0.26%	-0.69%	-0.26%	+0.15%	+0.29%	-1.32%
I_p	A	-1.14%	-1.65%	-2.25%	-2.01%	-3.24%	-4.06%
	B	-0.66%	-1.28%	-2.07%	-1.42%	-2.87%	-3.33%
	C	-0.22%	-1.63%	-0.91%	+1.10%	+0.26%	-1.17%
V_s	A	-0.31%	-0.24%	-0.40%	-0.32%	+0.17%	-0.86%
	B	-0.55%	-0.46%	-1.05%	-1.24%	-1.41%	-2.04%
	C	-0.06%	+0.12%	-0.26%	-0.43%	-0.06%	-0.79%
I_s	A	-0.43%	-0.67%	-0.55%	-0.23%	-0.42%	-1.49%
	B	-0.43%	-0.48%	-1.25%	-0.86%	-1.24%	-2.82%
	C	-0.24%	+0.39%	-0.41%	+0.92%	+0.88%	-0.02%

Table 2: Experimental results for voltages and currents on primary and secondary side, in terms of symmetrical components - variations with respect to rated load test (reference).

Number of Lost Turns		1		2		3	4
Test		1 - 2	2 - 3	1 - 3	3 - 5	2 - 5	1 - 5
V_p	D	-0.56%	-2.59%	-0.54%	-2.23%	-1.60%	-1.12%
	I	+101.64%	+310.03%	+64.98%	+184.87%	+265.97%	+62.97%
	H	+78.69%	+240.85%	+60.95%	+171.60%	+220.11%	+45.57%
I_p	D	-1.09%	-3.10%	-1.67%	-2.24%	-2.76%	-3.02%
	I	+110.33%	+370.85%	+74.65%	+195.80%	+294.10%	+22.59%
	H	+44.80%	+181.07%	+10.61%	+121.73%	+171.29%	+12.27%
V_s	D	-0.91%	-1.56%	-1.30%	-2.72%	-2.36%	-2.14%
	I	+50.27%	+97.86%	+51.42%	+39.81%	+127.58%	+55.28%
	H	+49.48%	+80.44%	+54.12%	+56.82%	+113.06%	+74.06%
I_s	D	-1.11%	-1.63%	-1.51%	-2.15%	-2.07%	-2.33%
	I	+62.26%	+106.06%	+48.77%	+53.24%	+140.58%	+64.97%
	H	44.78%	+79.34%	+57.63%	+51.07%	+111.30%	+71.46%

1. The loss of a greater number of coil turns is always more severe (for example, the loss of 2 turns is more severe than the loss of a single turn, regardless of fault location);

2. For the same number of lost coil turns, the fault becomes more severe as one moves downward in the coil, farther from the middle section and closer to the bottom extremity of the limb. This consideration is based on the simulation results of section 4.1, where it was established that the demagnetization of the iron core is stronger when the fault happens closer to one of the extremities of the limb.

As expected, by looking only at electrical variables, it is difficult to accurately locate faults within a given coil, since the effect of fault location is less evident in electrical variables than in magnetic quantities, as shown by the simulation methods described in section 4.1. However, if one is solely concerned with the detectability and severity of the fault in terms of the number lost turns, rather than its location, it is possible to obtain higher levels of accuracy. To illustrate this point, fault tests were grouped according to the number of lost turns and average severity ratings were taken for each group. The results are presented in tab. 4, where all vari-

ables from tab. 3 that showed an accuracy lower than 50% have been discarded.

Table 3: Severity rating of each fault test according to different electrical variables.

Method		Severity Rating						Accuracy
		1 - 2	2 - 3	1 - 3	3 - 5	2 - 5	1 - 5	
Reference		1	2	3	4	5	6	-
V_p	D	2	6	1	5	4	3	0%
	I	3	6	2	4	5	1	16.67%
	H	3	6	2	4	5	1	16.67%
I_p	B	1	2	4	3	5	6	66.67%
	D	1	6	2	3	4	5	16.67%
	I	3	6	2	4	5	1	16.67%
V_s	B	2	1	3	4	5	6	66.67%
	D	1	3	2	6	5	4	33.33%
	I	2	5	3	1	6	4	16.67%
	H	1	5	2	3	6	4	16.67%
I_s	B	1	2	5	3	4	6	50%
	D	1	2	3	5	4	6	66.67%
	I	3	5	1	2	6	4	0%
	H	1	5	3	2	6	4	16.67%

Table 4: Average severity rating of each fault test according to different electrical variables and number of lost coil turns.

Number of Lost Turns		Average Severity Rating						Accuracy
		1		2		3	4	
Method		1 - 2	2 - 3	1 - 3	3 - 5	2 - 5	1 - 5	
Reference		1.5		3.5		5	6	-
I_p	B	1.5		3.5		5	6	100%
V_s	B	1.5		3.5		5	6	100%
I_s	B	1.5		4		4	6	50%
	D	1.5		4		4	6	50%

In an attempt to gain accuracy in locating the faults within the winding, the magnetic flux density leakage between transformer limbs was also measured for the same set of tests, resorting to two hall effect probes. This method proved to be promising according to simulation results. However, experimentally, it was not possible to distinguish significant variations of the magnetic flux density leakage in the presence of faults. This might indicate that the conclusions of section 4.1 are not strictly scalable and depend on the volume and rated power of the transformer.

Finally, a temperature test was performed. To establish a baseline for comparison a rated load test was performed. Then, the fault corresponding to total loss of all rerouted turns (worst incipient fault possible with the current experimental setup) was also tested. The temperature was measured in the top section of the core, above each limb, using three thermal sensors located as shown in fig. 18. During each test, the transformer was left operating with its enclosure open until temperature stabilization was achieved. Table 5 shows the increase in core temperature caused by the presence of a fault, with respect to the reference test. Note that these values refer to the difference between core and ambient temperature, to account for calibration unbalances in the sensors.

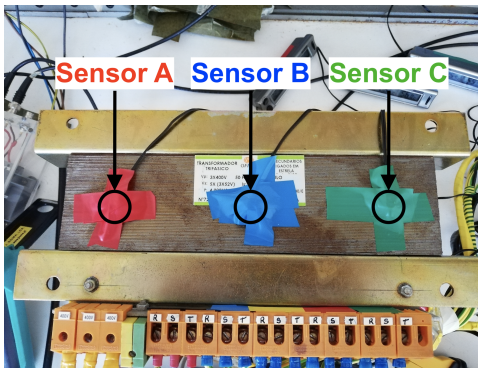

Figure 18: Location of thermal sensors on top section of the transformer core.

Table 5: Increase in temperature due to presence of incipient fault in middle limb.

	Left Limb	Middle Limb	Right Limb
Temperature Increase	17.74%	18.75%	15.87%

These results indicate not only that the presence of an incipient fault might cause core temperature to increase greatly, but also that, as expected, said increase will potentially be more significant in the limb where the fault occurs. This can be explained by the demagnetization of the core and consequent redistribution of magnetic flux density due to the presence of an incipient fault in the middle limb.

However, note that this conclusion should be subjected to further study, since only a limited number of tests were performed.

5. Conclusions

5.1. Achievements

In this work, a 2D FEM model was developed, which is able to perform quick frequency domain simulations at relatively low computational cost, while providing satisfactorily accurate results. It was possible, based on these results, to establish a potential methodology for incipient fault detection and localization in distribution transformers. This methodology is valid for faults in the secondary and can be applied to the primary winding to some extent.

The experimental setup built in the laboratory gave a deeper insight regarding the variables here studied and the scalability of the proposed methodology regarding transformer geometry and power.

5.2. Future Work

For future work, the following guidelines should be considered:

- Simulation of transformer behavior with typical varying load profiles to approximate the operating conditions of field units;

- Performance of 2D simulations for multiple geometries and rated voltage/current levels in order to assess the scalability of the proposed methodologies;

- Discretization of the magnetic leakage flux measurement method to approximate sensor installation and improve localization capabilities;

- Development of a 3D simulation model, to account for non-uniform distribution of magnetic flux density and enable the simulation of the thermal behavior of the transformer;

- Injection of data gathered from field units by Eneida Wireless & Sensors, S.A., in the aforementioned 3D model and assessment of hotspot locations;

Acknowledgements
The author would like to acknowledge Prof. Paulo José da Costa Branco for supervising of this work and the team of Eneida Wireless & Sensors, S.A., for making it possible.

References

[1] S. Meijer, M. D. Judd, and S. Tenbohlen. Sensitivity check for radio frequency partial discharge detection for power transformers. In *International Conference on Condition Monitoring and Diagnosis, Beijing, China*, April 2008.

[2] E. Helera. Power transformer incipient faults monitoring. *Annals of the University of Craiova, Electrical Engineering Series*, 32, 2008. ISSN 1842-4805.

[3] D. Marcsa. Noise and vibration analysis of a distribution transformer. *Przeglad Elektrotechniczny*, 1(12):174–177, December 2019.

[4] V. Nurmanova, A. Sultanbek, M. Bagheri, R. A. Ahangar, O. Abedinia, T. Phung, and G. B. Gharehpetian. Distribution transformer frequency response analysis: Behavior of different statistical indices during inter-disk fault. In *IEEE International Conference on Environment and Electrical Engineering and IEEE Industrial and Commercial Power Systems Europe (EEEIC / I&CPS Europe)*, 2019.

[5] Y. Gao. *Assessment of Future Adaptability of Distribution Transformer Population Under EV Scenarios*. PhD thesis, University of Manchester, Faculty of Engineering and Physical Sciences, School of Electrical and Electronic Engineering, 2016.

[6] S. Chaudhary. *Condition Monitoring Techniques of Power Transformers*. Triveni Engineering & Industries Ltd., Deoband, Saharanpur, Uttar Pradesh, India, October 2017.

[7] L. Cheim, D. Platts, T. Prevost, and S. Xu. Furan analysis for liquid power transformers. *IEEE Electrical Insulation Magazine*, 27(6):29–42, November 2011.

[8] M. Wang, A. J. Vandermaar, and K. D. Srivastava. Review of condition assessment of power transformers in service. *IEEE Electrical Insulation Magazine*, 18(6):12–25, November / December 2002.

[9] M. Ohlen and P. Werelius. *A Guide to Transformer Ratio Measurements*. Megger Sweden AB, 187 29 Täby, Sweden, January 2010.

[10] B. Hembroff, M. Ohlen, and P. Werelius. *A Guide to Transformer Winding Resistance Measurements*. Manitoba Hydro and Megger Sweden AB, April 2010.

[11] Omicron Energy. *Diagnostic testing and monitoring of power transformers*, March 2020.

[12] M. J. Mousavi and K . L. Butler-Purry. Transformer internal incipient fault simulations. January 2003.

[13] L. M. R. Oliveira and A. J. M. Cardoso. Online diagnostics of transformer winding insulation failures, by Park's vector approach. In *Proceedings of the 9th International Electrical Insulation Conference (INSUCON 2002), Berlin, Germany*, pages 16–21, June 2002.

[14] K. L. Butler-Purry and M. Bagriyanik. Identifying transformer incipient events for maintaining distribution system reliability. In *Proceedings of the 36th Hawaii International Conference on System Sciences*. IEEE, February 2003.

[15] S. Tenbohlen, M. Siegel, and M. Beltle. Partial discharge monitoring of power transformers by UHF sensors. In *ARWtr2016 - Advanced Research Workshop on Transformers, La Toja Island, Spain*, October 2016.

[16] M. T. Ishak and Z. Wang. Transformer hotspot temperature calculation using IEEE loading guide. In *International Conference on Condition Monitoring and Diagnosis, Beijing, China*, April 2008.

[17] Z. Radakovic, E. Cardillo, and K. Feser. Temperature distribution in windings of transformers with natural oil circulation. January 2002.

[18] G. Rigatos, P. Siano, and A. Piccolo. Incipient fault detection for electric power transformers using neural modeling and the local statistical approach to fault diagnosis. In *2012 IEEE Sensors Applications Symposium Proceedings*, pages 1–6, 2012.

[19] B. Das, S. Janssens, and S. Raymond. Distribution transformer hot spot temperature monitoring based on fbg sensors. In *EEA Conference & Exhibition, Wellington*, June 2015.

[20] L. Wang, Q. Wang, W. Qin, T. Liao, H. Yag, and G. Ma. Temperature monitoring of distribution transformer windings based on fiber bragg grating array. In *2nd International Conference on Electrical Materials and Power Equipment (ICEMPE), Guangzhou, China*, 2019.

[21] S. Guo, K. Long, Z. Hao, J. Ma, H. Yang, and J. Gan. The study on vibration detection and diagnosis for distribution transformer in operation. In *China International Conference on Electricity Distribution (CICED 2014), Shenzhen*, pages 983–987, September 2014.

[22] N. Vieira, C. Martins, G. Dias, A. Coelho, and P. Antunes. Vibro-acoustic analysis of a distribution power transformer using the finite element method. In *CWIEME 2008 - Coil Winding, Insulations & Electrical Manufacturing, Berlin, Germany*, June 2008.

[23] J. Jagers and S. Tenbohlen. Differences approaches for the acquisition of reliability statistics. In *CIGRE Regional Conference*, 2009.

[24] A. Dente. Sistema Electromecânicos I, Cap. 3: Transformadores. Sebenta de Apoio à UC de Máquinas Elétricas, Instituto Superior Técnico, 2004.

[25] COMSOL. *AC/DC Module User's Guide*. page 309.

[26] P. Bhagubai. Otimização multiobjectivo do núcleo de uma máquina elétrica usando uma liga de vanádio-cobalto. Master's thesis, Universidade de Lisboa: Instituto Superior Técnico, June 2019.